Hindawi
Advances in Civil Engineering
Volume 2020, Article ID 8831506, 14 pages
https://doi.org/10.1155/2020/8831506

Research Article

Numerical Simulation of Pervious Concrete Based on Random Pore Model

Jingsong Shan,[1] **Jinle He**,[1] **and Feng Li**[2]

[1]*Shandong Key Laboratory of Civil Engineering Disaster Prevention and Mitigation, Shandong University of Science and Technology, Qingdao 266590, China*
[2]*Shandong Huitong Construction Group Co., Ltd, Jinan 250002, China*

Correspondence should be addressed to Jingsong Shan; cyhsjs@163.com

Received 10 May 2020; Revised 3 July 2020; Accepted 15 July 2020; Published 4 August 2020

Academic Editor: Xue Zhang

The features of the pores in pervious concrete have a great influence on the mechanical property of the pervious concrete. In this study, a finite element model (FEM) with random pores has been used to simulate the mechanical characteristics of pervious concrete. First, pervious concrete specimens with two different porosities were prepared in the laboratory. Then, the specimens were cut and the pores features were extracted based on the images of cross-sections. Thereafter, the ellipse and roundness were introduced into a simulation model to describe the characteristics of pores including the size, area, shape, and inclined angle which have been developed randomly in the FEM using the Monte Carlo method. In the simulation model, the aggregate and cement paste have been simplified into a composite material, and the method of determining the composite modulus of aggregate-cement paste is discussed. The simulation results show that the shape and distribution of the pores have an obvious influence on the internal stress of the pervious concrete and the pore features can be considered reasonable for the validity of the simulations. In addition, the composite modulus of the aggregate-cement paste can be determined by comparing the simulation and test results. The recommended composite modulus in the pervious concrete simulation model is much lower than that of common impervious concrete.

1. Introduction

Pervious concrete is material that has been used to favor the permeability of surfaces. The most singular characteristic that favors the selection of this special type of concrete is its interconnected porosity. There are many earlier studies on the pore feature and numerical simulations of pervious concrete. They found that there is a close correlation between porosity, permeability, and mechanical properties of pervious concrete. In the studies of Debnath and Sarkar [1] and Tang et al. [2], they found that the presence of fine aggregates hindered the formation of pores, and the single size aggregate could increase the permeability. The porosity and pore features of pervious concrete are important to the permeability and mechanical properties [3]; thus, porosity ranging from 15% to 25% was recommended [4]. Crouch et al. [5] pointed out that the larger the aggregate particle size within a given range was, the more effective the size of the pore formed was. Similarly, in the literature [6, 7], they found that aggregate size was the main factor affecting porosity, and the water-cement ratio was a secondary influencing factor.

There are two main methods to determine the pore structure of pervious concrete. One is to use the nondestructive test method by combining tomography and digital image processing [2, 3, 8–11]. Many researchers used this method to extract and analyze the pore characteristics of pervious concrete. The second method is to measure the total porosity by the volumetric test and extract the pore features from the planar images. In the latter method, specimens of pervious concrete need to be cut before the test. Martin et al. [12] developed a method for measuring porosity distribution using image analysis techniques. Rehder et al. [13] also used this method to investigate the relationship between pervious

concrete cracking and pore characteristics. Similarly, Zhong and Wille [14] and Sumanasooriya and Neithalath [7] used the method of volume and image analysis to describe the pore distribution of pervious concrete.

Pervious concrete is a multiphase material. Both the experimental and numerical analyses were used to investigate mechanical properties of pervious concrete [15–20]. In a numerical model, reasonable consideration of pores and aggregate characteristics is very important. Mohamed et al. [20–22] developed a random aggregate model to simulate the random distribution of multigrade aggregates which can determine an aggregate distribution that is satisfactory for common concrete. To improve the computing efficiency, the literatures [23–25] simplified the shape of an aggregate to a spherical shape and converted the three-dimensional model into a two-dimensional model for numerical simulations. Using the finite element method (FEM), Schlangen and van Mier [26] and Van Mier [27] developed a grid model for the first time to simulate the failure process of pervious concrete. In the simulation model, the material properties can be directly assigned and the mechanics of pervious concrete can be simulated.

The above literature review shows that the method of random distribution aggregate model was usually used in the earlier studies. But the cement paste layers between the aggregates were difficult to define for pervious concrete because of the small thickness. In addition, there are a large number of macropores in pervious concrete which should not be ignored. In this study, using the random pore distribution method, a different way has been used to develop a numerical model. First, the pore image data of pervious concrete have been extracted from the cut specimen of the pervious concrete. Then, the pore features have been analyzed by digital image processing technology. Based on the pores characteristics, the random generation of pores has been programmed in the development of the pervious concrete simulation model.

2. Experiment and Method

2.1. Raw Materials

2.1.1. Cement. In accordance with the requirements of the Chinese specification CJJT135-2009 [28], Portland cement with a strength grade 42.5 MPa has been used. The detailed quality parameters are listed in Table 1.

2.1.2. Coarse Aggregate. Two sizes of aggregate have been used in this study which was obtained from the local quarries in Shandong province of China. The two sizes are D1: 4.75–9.5 mm and D2: 9.5–13.2 mm basalt (Figure 1) which have been mixed according to the mass percentage, D1 (80%): D2 (20%). The characteristics are listed in Table 2.

2.2. Preparation of Specimens. Related studies have shown that the porosity of pervious concrete meeting both strength and permeability is generally between 20% and 30%. Thus, 22% and 28% have been selected as the designed porosity in the test, representing the lower and higher porosities, respectively. The two types of specimens have been labeled as 1# and 2#. According to the designed porosities, the amounts of raw materials per unit volume have been determined, as shown in Table 3.

Six 100 mm cubic specimens for each designed porosity were prepared as follows. The quantities of material according to the composition in Table 3 were prepared. They were then put into a forced mixer and mixed by the cement-coated stone method (Figure 2(a)). Thereafter, the mixture was poured into a mold and compacted by a heavy hammer (Figure 2(b)) [29]. Finally, the specimens were removed from the molds after 24 hours and cured for 28 days (Figures 2(c) and 2(d)). Parts of the cured specimens were cut and the pore features were measured. The other parts of the cured specimens were used in the measurements of the mechanics including stress-strain curve and compressive strength.

2.3. Porosity Measurement of Prepared Specimens. The volumetric method has been used to calculate the void content and the connected porosity of the prepared specimens. Firstly, the mass of the cured pervious concrete specimen in water was measured. Then, the specimens were placed in a drying box and the mass was measured after drying. Finally, the bulk volume of specimen was measured by a vernier caliper. Using equations (1)–(3), the total void ratio and the connected void ratio have been determined:

$$\rho_t = \frac{100 + p_c + 0.25p_c}{(100/\rho_a) + (p_c/\rho_c) + ((1/4)\cdot(3/4)\cdot p_c)}, \quad (1)$$

$$n_0 = \left(1 - \frac{\rho_s}{\rho_t}\right) \times 100\%, \quad (2)$$

$$n_e = \left(1 - \frac{m_2 - m_1}{v \cdot \rho_w}\right) \times 100\%, \quad (3)$$

where ρ_t is theoretical density of the pervious concrete materials; n_0 is the void content; n_e is the connective porosity; p_c is the mass ratio of cement to coarse aggregate; ρ_a is the apparent density of coarse aggregate; ρ_c is the apparent density of cement; ρ_s is the gross bulk density of pervious concrete; m_2 is the dry mass of the specimen; m_1 is the mass of the specimen in water; ρ_w is the density of water; and v is the volume of the specimen.

2.4. Pore Extraction. The cubic specimens were cut vertically and a high-definition digital camera was used to obtain the cross-sectional image. In the process of image acquisition, the quality of digital image was often affected by some noise, such as the camera quality and lighting. In order to improve the image quality, the cut section image needs to be enhanced. The original image was therefore processed by the software PSCC based on the smoothing and sharpening algorithm in the spatial domain. Taking the specimen with the 22% designed porosity as an example, the test specimen

Table 1: Cement quality parameters.

Test items	Consistency (mm)	Initial setting time (min)	Final setting time (min)	Compressive strength (MPa)	
				3 days	28 days
Material parameters	28	150	250	24.7	47.2

(a) (b)

Figure 1: Coarse aggregate: (a) particle size 4.75 mm~7.5 mm; (b) particle size 9.5 mm~13.2 mm.

Table 2: Coarse aggregate properties.

Aggregate	Bulk density (kg/m^3)	Apparent density (kg/m^3)	Void in mineral aggregate (%)
D1	1643	2819	40.32
D2	1611	2855	41.35
D1 (80%): D2 (20%)	1622	2830	41.17

Table 3: Compositions of pervious concrete.

Specimens group	Design porosity (%)	Coarse aggregate (kg/m^3)	Cement (kg/m^3)	Water (kg/m^3)
1#	22	1631.7	417.2	125.1
2#	28	1631.7	319.6	95.9

was vertically cut into a 100 mm square. The original image and the enhanced image are shown in Figure 3.

To obtain the pore information from the enhanced image, the steps are as follows:

(1) Select a reasonable threshold to segment the enhanced image.

(2) Compare the threshold with the gray value of pixels in the image: if the gray value of the pixel area is higher than the threshold, the area is marked 1; otherwise it is marked 0.

(3) Import the binarized image into the software Image-Pro Plus, and set the scale parameters to calculate the planar pore characteristics in the digital image.

The binarized image and planar pore characteristic parameters are shown in Figure 4.

2.5. Pores Characteristics. The pores structural characteristics mainly include three aspects: porosity, pore size, and pore shape.

2.5.1. Planar Porosity. A single pore area can be obtained by counting the number of pixels in the pore. All the pore areas can be obtained by calculating the sum of all the pore pixels in the section image. The planar void ratio is the ratio of all the pore areas to the cross-sectional area. Because the unit in the software Image-Pro Plus is pixels, used to describe the

(a) (b) (c) (d)

Figure 2: Pervious concrete specimen preparation: (a) mixing; (b) compact; (c) molded specimens; (d) curing.

(a) (b)

Figure 3: Digital image of cut section: (a) original 2D digital image; (b) enhanced 2D digital image.

digital image, it is necessary to convert the pore pixel data to an area unit. By adjusting the digital image to 1000×1000 pixels, the pore area in mm^2 can be calculated as follows:

$$\text{Pore area}\left(mm^2\right) = \text{Pore area}\left(\text{pixel}^2\right) \cdot \frac{100 \times 100\,mm^2}{1000 \times 1000\,\text{pixel}^2}, \tag{4}$$

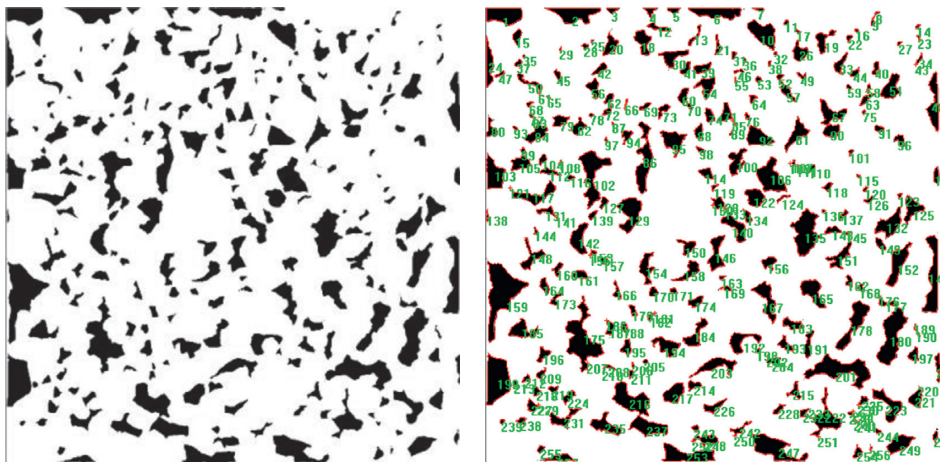

(a) (b)

Figure 4: Planar pores extraction from cut section image: (a) binarized image; (b) pores feature parameters extraction.

2.5.2. Planar Pore Shape. To facilitate the description of the pore morphology, the pores are simplified to a circular and an elliptical shape as described by the equivalent diameter and roundness, respectively. The equivalent diameter (D_e) of a single pore is calculated as follows:

$$\text{Equivalent diameter} = 2 \cdot \left(\frac{\text{Pore area}}{\pi}\right)^{1/2}. \quad (5)$$

The pore shape of an ellipse is defined by the roundness which is the ratio between the long and short axis of an equivalent ellipse (Figure 5). When the roundness value of the pore is close to 1, it means the shape of the pore is close to a circle. On the other hand, if the value of pore roundness is far from 1, it means the difference between the long axis and the short axis is large and the shape of the pore is elongated. The roundness is calculated as follows:

$$\text{Roundness} = \frac{\text{Length of long axis}}{\text{Length of short axis}}. \quad (6)$$

2.6. Random Pores FEM. To analyze the influence of pores on the mechanical properties of pervious concrete, the aggregate-cement is assumed to be a homogeneous material in the simulation model and the pores are randomly distributed among aggregate-cement materials. The pore characteristics, such as size, shape, and porosity, are determined according to the actual data from the image analysis data. The steps for developing a FEM of pervious concrete are as follows:

(1) Analyze the pore structural characteristic including the equivalent diameter and long axis and short axis radius of an elliptical pore and the pore area. Further, the pores are divided into several groups based on the equivalent diameter.

(2) The pores are randomly generated for every group, and the size, position, and angle of the pores are determined randomly within the set range.

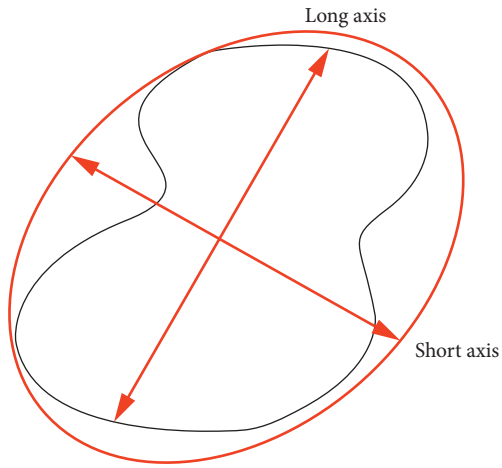

Figure 5: Schematic diagram of pore shape.

(3) The effectiveness need to be verified when one pore is generated. If the new pore overlapped with an existing pore, the newly generated pore is invalid and deleted. This process of pore generation is repeated until the new pore did not intersect with any of the existing pores. When the total areas of the generated pores reach a predetermined value, the process of pore generation is stopped.

(4) All the pores areas are subtracted from the model region by the Boolean operation in the finite element software Ansys to generate a two-dimensional model with random pores.

(5) Apply the boundary conditions, material properties, and load conditions to solve.

Taking the cross-sections of the specimens with 15% and 20% porosities as examples, the random circular pores and the random elliptical pores generated by the finite element model are, respectively, shown in Figures 6 and 7.

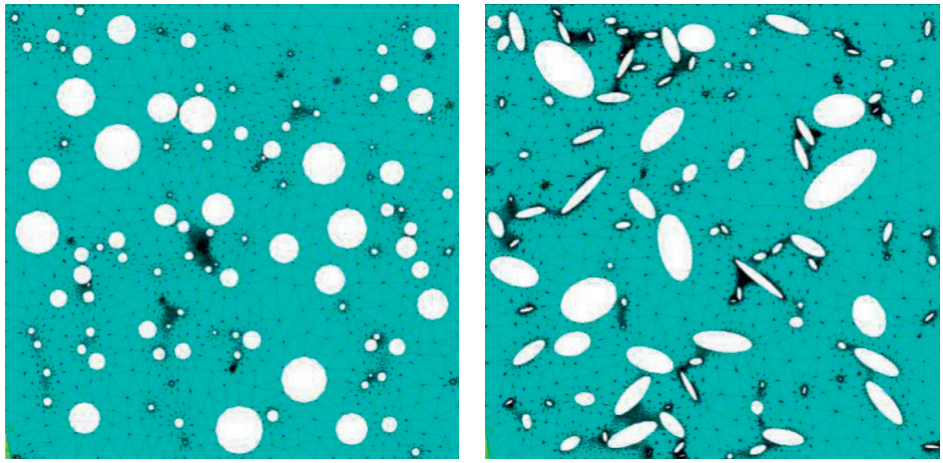

(a) (b)

Figure 6: Finite element model with planar porosity of 15%: (a) random circular pores; (b) random ellipse pores.

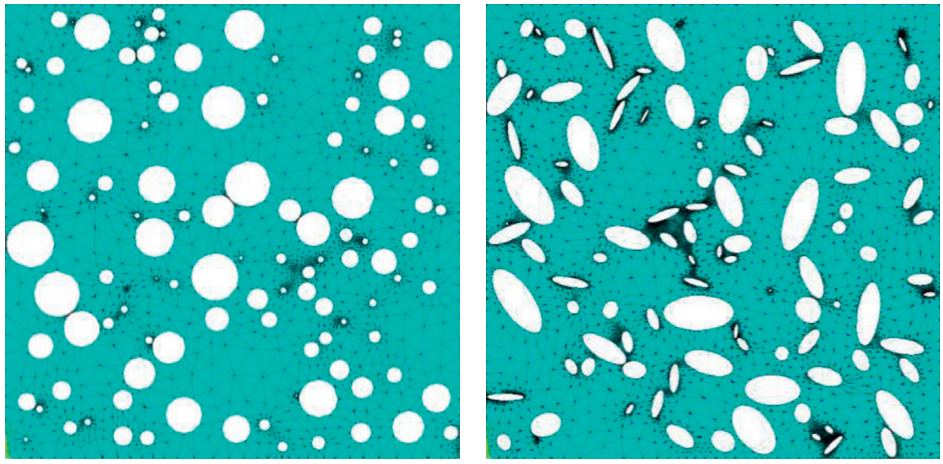

(a) (b)

Figure 7: Finite element model with planar porosity of 20%: (a) random circular pores; (b) random ellipse pores.

2.7. Compressive Test. The compressive strength of the specimens was tested at the age of 28 days in accordance with ASTM C39-15a and Chinese specification CJJT135-2009. The loading rate is 1 mm/min and the compressive force was applied until the specimen displayed a well-defined fracture pattern. During the compressive test, the load magnitude and deformation were recorded at the same time by a control computer (Figure 8).

3. Results and Discussion

3.1. Porosity of Pervious Specimens. In Table 4, the void content of the specimens is close to the designed porosity for specimens 1# and 2#. The void content includes closed pores and connective pores in which the permeability of pervious concrete is mainly affected by the connective pores. The average connective porosity is 16.7% making up 71.6% of void content for specimen 1#. On the other hand, the average connective porosity accounts for 93.4% in specimen 2#. Thus, with the increase in the designed porosity, the ratio of the connective pores to void content clearly increases. This is due to the bridging of the cement paste between the aggregate particles. When the designed porosity is lower, more cement paste is required to fill the voids between the aggregate particles and many pores are also sealed in the net of the cement paste. On the other hand, to meet the porosity requirement when the designed porosity is higher, the quantity of cement paste required to be added to the mixture is much smaller. In this case, the cementitious paste layer surrounding the coarse aggregate is thinner and hard to form sufficiently closed voids.

3.2. Planar Pore Features and Distribution. According to the pore data extracted from the section image of the pervious concrete, both the equivalent diameter and the roundness of the pores have been calculated and analyzed. The results show that the equivalent diameter ranges from 0 to 10 mm

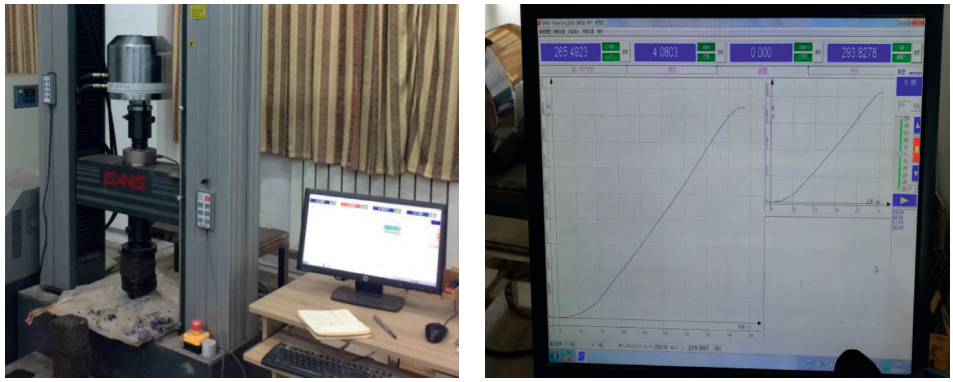

(a) (b)

Figure 8: Compressive test control system: (a) compression test machine; (b) compression test control computer.

Table 4: Volume parameters of specimens.

	Specimen number	Design porosity (%)	Void content (%)	Average void content (%)	Connective porosity (%)	Average connective porosity (%)	Specimen volume (mm^3)
1#	1-1	22	22.0	21.8	16.8	16.6	1015
	1-2		22.3		16.3		1012
	1–3		21.5		16.9		1014
	1–4		22.6		17.1		1013
	1–5		21.0		16.5		1005
	1–6		21.5		16.2		1008
2#	2-1	28	27.0	27.3	25.2	25.5	1010
	2-2		27.6		25.8		1012
	2-3		27.3		25.7		1012
	2–4		26.9		25.0		1010
	2–5		27.4		25.5		1009
	2–6		27.6		25.8		1007

for specimen 1# and ranges from 0 to 13 mm for specimen 2# (Figure 9). There are more pores when the equivalent diameter is smaller and the number of pores decreases with increasing equivalent diameter. The equivalent diameter of most pores is smaller than 5 mm in specimen 1# and smaller than 7 mm in specimen 2#.

In Figure 10, the variation of the number of pores with the roundness is plotted and the results show that the roundness of the pores varies from 0 to 7 for specimens 1# and 2#. The number of pores decreases with increasing roundness. It is noted that the roundness less than 3 accounts for more than 80% of all pores, which means that the shape of most pores is close to circular and only a small number of pores are slender.

For the subsequent simulation models, the pores have been divided into five groups based on the equivalent diameter (D_e), i.e., tiny pores ($D_e \leq 1.0$ mm), small pores ($D_e = 1.0 \sim 2.5$ mm), medium pores ($D_e = 2.5 \sim 5.0$ mm), large pores ($D_e = 5.0 \sim 9.0$ mm), and super pores ($D_e \geq 9.0$ mm). Accordingly, the lengths of long axis and short axis of the pores have been extracted and sorted, as shown in Tables 5 and 6. The results show that the sum of the areas with large pores is the largest followed by the areas with super pores and then the areas with medium pores. The areas with tiny pores and small pores are remarkably lower than the areas with bigger pores even though the numbers of tiny pores and small pores are much bigger.

3.3. Simulation of Pervious Concrete

3.3.1. Verification of Numerical Simulation Models. To verify the random pore models, the size, area, and number of pores in each group have been recorded by a program in the process of pores generation. The recorded statistical data have been used to verify whether the porosity in the FEM is consistent with reality. The comparisons are shown in Table 7. The results show that the generated pores for the five groups of pores are all close to the actual porosities. Thus, the method of random pore FEM can be used to develop an accurate model reflecting the actual pore features and distributions in pervious concrete. However, it should be noted that the actual pores have been simplified into circles or ellipses according to the shape and size of the real pores. This may cause some differences between the simulation and the real response of the pervious concrete. However, the computing efficiency is greatly improved.

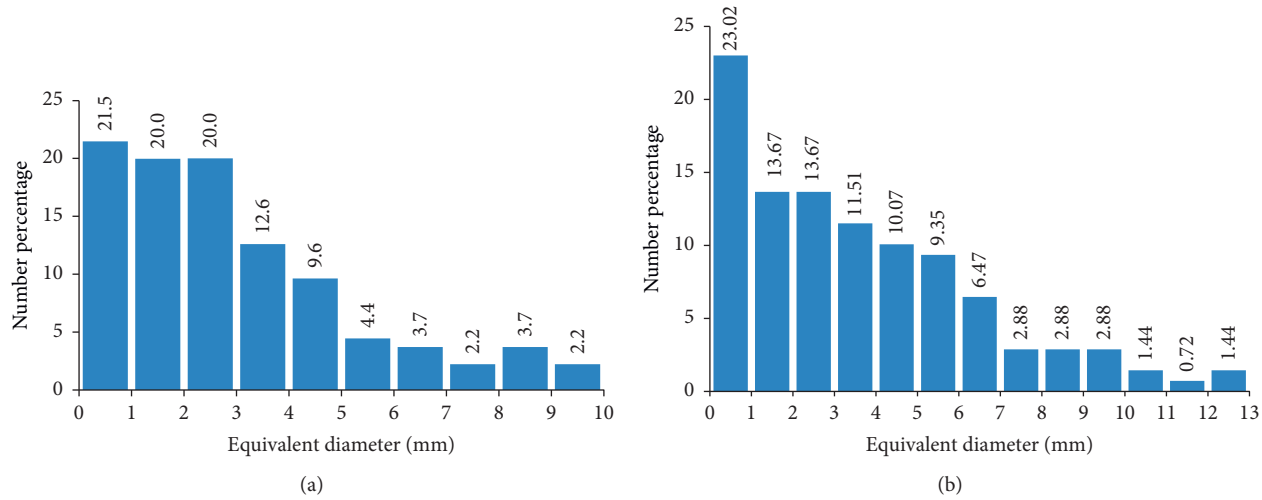

Figure 9: The number of pores with different equivalent diameter: (a) specimen 1#; (b) specimen 2#.

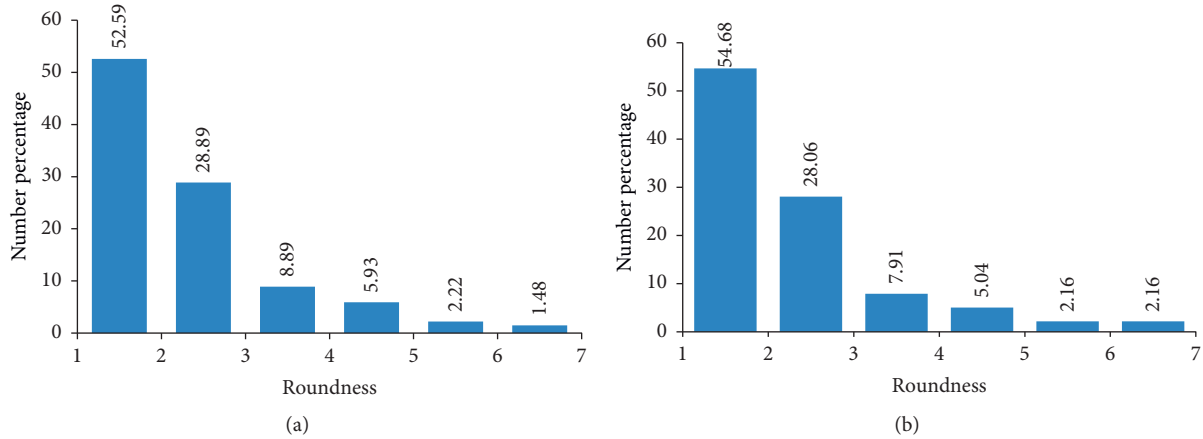

Figure 10: The number of pores with different roundness: (a) specimen 1#; (b) specimen 2#.

Table 5: Statistical results of pores feature for specimen 1#.

Parameter	Range				
	Tiny pores	Small pores	Medium pores	Large pores	Super pores
Equivalent diameter (mm)	<1.0	1–2.5	2.5–5	5–8	>9
Long axis range (mm)	0.15–1.9	1.2–3.6	3–9	7.6–13	12.6–20
Short axis range (mm)	0.12–0.75	0.74–2	1.3–3.4	2–8	5.4–9.6
Planar porosity (%)	0.07	1.2	3.05	5.8	4.1

Table 6: Statistical results of pores feature for specimen 2#.

Parameter	Range				
	Tiny pores	Small pores	Medium pores	Large pores	Super pores
Equivalent diameter (mm)	<1.0	1–2.5	2.5–5	5–8	>9
Long axis range (mm)	0.15–1.02	1.3–3.8	3–8.4	5.8–13	12–18
Short axis range (mm)	0.1–0.75	0.7–1.8	1.4–4.4	1.9–7	5–8.4
Planar porosity (%)	0.01	0.6	5.5	9.4	6.1

Table 7: Porosity comparison between FEM and reality.

Parameter pores		Range				
		Tiny pores	Small pores	Medium pores	Large pores	Super pores
Specimen 1#	Actual porosity (%)	0.07	1.2	3.05	5.8	4.1
	Circular pore model (%)	0.07	1.12	3.07	5.95	4.10
	Ellipse pore model (%)	0.07	1.14	3.14	6.01	4.11
Specimen 2#	Actual porosity (%)	0.01	0.6	5.5	9.4	6.1
	Circular pore model (%)	0.01	0.60	5.53	9.57	6.51
	Ellipse pore model (%)	0.01	0.62	5.6	9.61	6.6

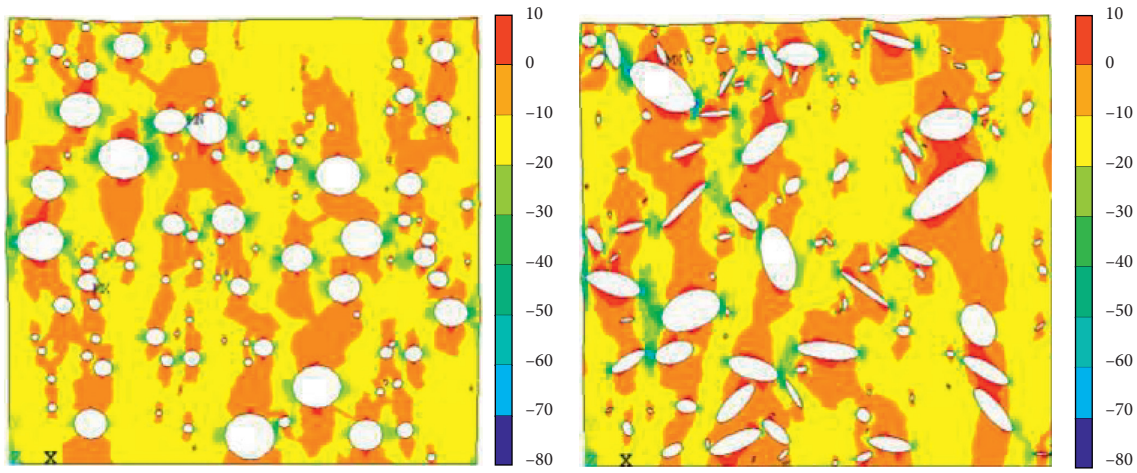

(a) (b)

Figure 11: Stress cloud in simulation model for specimen 1#: (a) random circular pores model; (b) random ellipse pores model.

3.3.2. Simulation Results

(1) Internal Stress Characteristics. In the simulation model, the vertical load was applied sequentially until failure of the specimens. With the increase in loading, the stress and strain in the simulation model increase linearly and the stress clouds results are shown in Figures 11 and 12. The results show that the internal stress is mainly compressive stress in the vertical direction, but tensile stress exists at the top and bottom of the pores. Since the tensile strength of concrete is weak, the regions near the top and bottom of the pores may crack first as induced by the tensile stress. In addition, the compressive stress on the left and right sides of the pores is much greater than the other regions in the model. The magnitude of the stress around the pores is affected by the pores spatial distribution. When the pores are aligned transversely and the distances between them are small, the vertical compressive stress will become larger between the pores. In this case, the effective bearing area between the pores is relatively small and distress may appear as induced by the compressive action. Similarly, if two pores are aligned vertically and the distance between them is small, the horizontal tensile stress may become larger between the pores. In this case, distress may appear as induced by the tensile action between the pores.

(2) Influence of Material Parameters. In the simulation model, the mixture of the aggregate-cement paste has been regarded as one composite material. The material parameter set in the FEM directly affects the mechanical properties of the pervious concrete. In this simulation, the composite elastic modulus of the aggregate-cement material has been used and set as a variable ranging from 2,000 to 20,000 MPa (Figure 13). The results show that the composite modulus of the aggregate-cement has a significant influence on the stress-strain of the pervious concrete. The slope of the stress-strain curves decreases with decreasing composite elastic modulus. For example, when the composite elastic modulus varies from 20000 to 5000 MPa, the slope of the stress-strain curves changes from 8928 to 2232 MPa for specimen 1# and 6578 to 1645 MPa for specimen 2#. The slope can be regarded as the overall modulus of the pervious specimens including the aggregate-cement paste and void. Thus, the results in Figure 13 also indicate that overall modulus of the pervious specimens is significantly lower than the composite modulus of the aggregate-cement paste material. This result

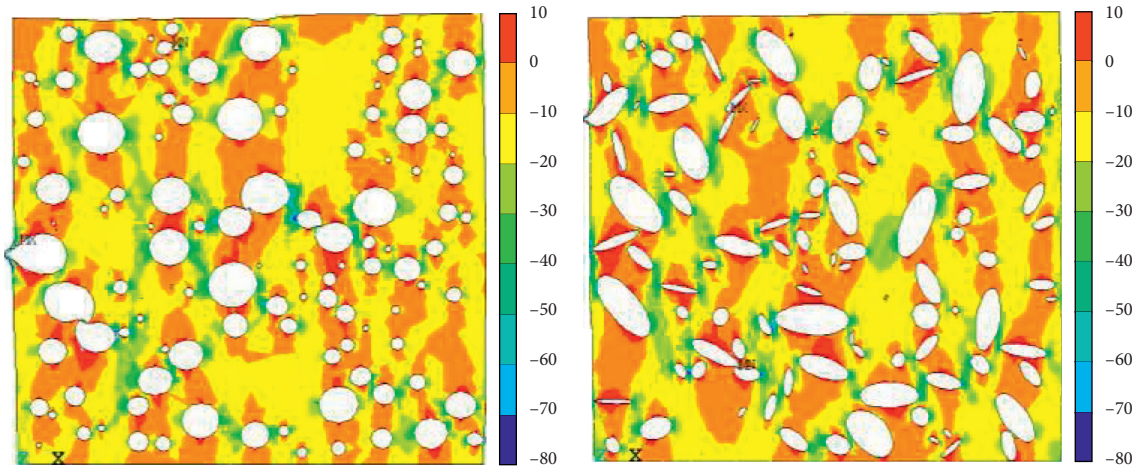

Figure 12: Stress cloud in simulation model for specimen 2#: (a) random circular pores model; (b) random ellipse pores model.

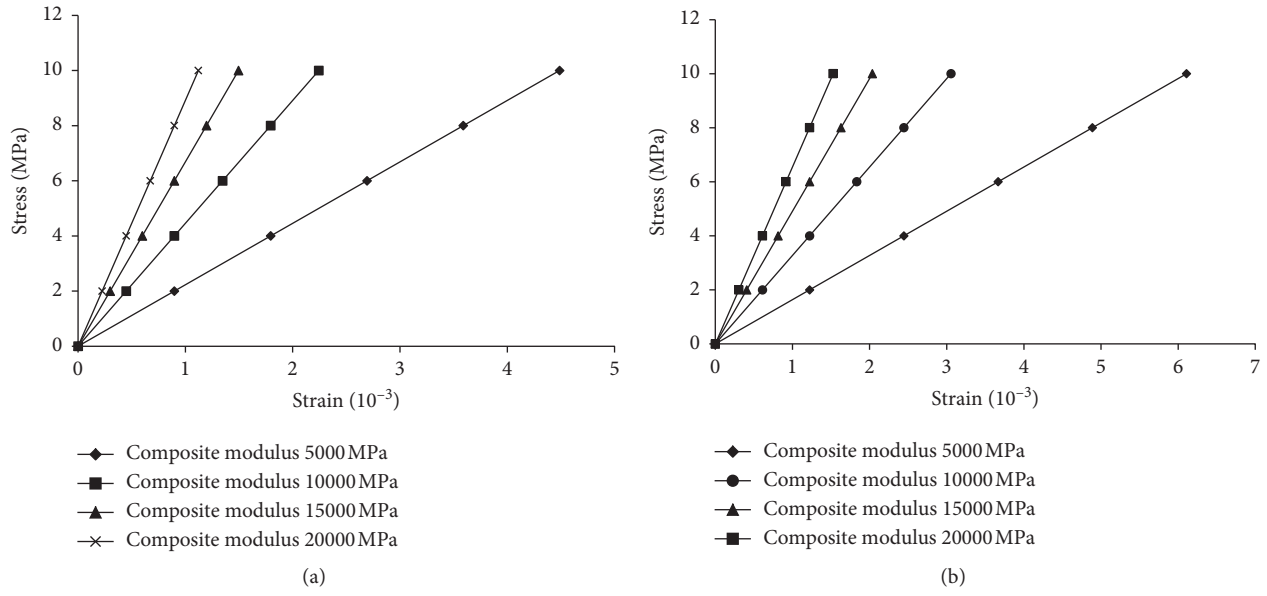

Figure 13: Variation of stress-strain curve of simulation model with composite modulus of aggregate-cement paste material: (a) specimen 1#; (b) specimen 2#.

is expected, as the existing pores weaken the pervious concrete, thereby reducing its ability of resisting loads.

(3) Influence of Pore Shape. To analyze the influence of pore shape from the simulation results, the material parameters have been set to constants in the simulation models. In Figure 14, the composite modulus of the aggregate-cement paste has been set to 5000 MPa and the shape of the pores has been simplified in a circle or an ellipse. The simulation results indicate that the differences between the two pore shapes are as follows. The compressive strain in the elliptical pore model is larger than that in the circular pore model. For example, in Figure 14(a), when the compressive stress reaches 10 MPa, the corresponding strain is 4.1×10^{-3} and 3.5×10^{-3} for the elliptical pore model and the circular pore model, respectively. This may be caused by the random distribution of the angle and the roundness of the elliptical pores, which can easily result in stress concentration surrounding the pores, especially around the flat pores. So, it is necessary to consider the pore shape in the simulation model of pervious concrete. Certainly, the pore features should be evaluated fully based on the actual specimens before developing the simulation model.

3.4. Determination of Composite Modulus of Aggregate-Cement Paste

3.4.1. Test Results of Mechanical Property. With the increase in the loading force, an increase of deformation was measured during the compressive test in the laboratory.

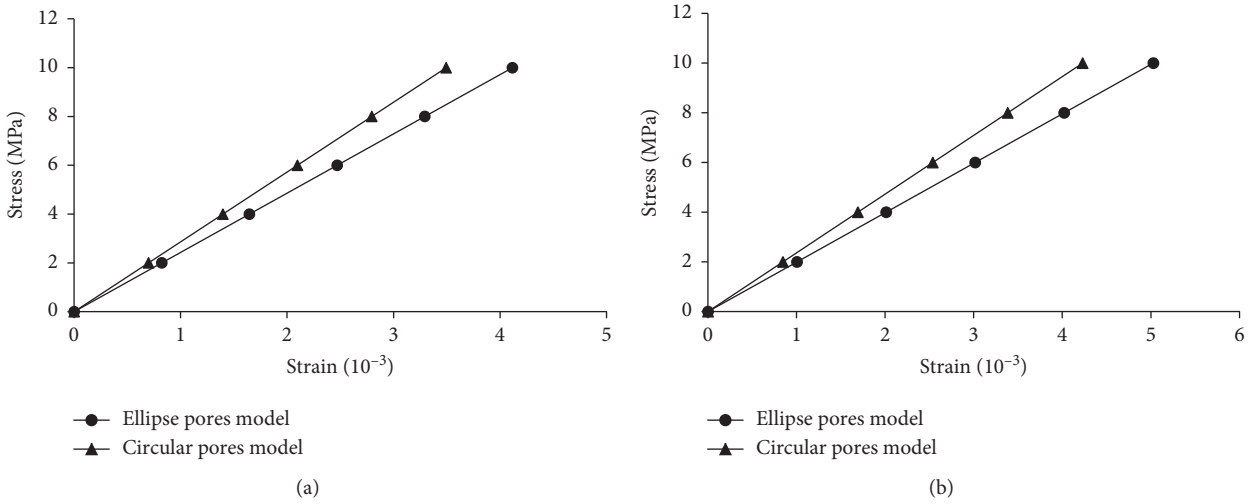

Figure 14: Effect of pores shape on the simulation results: (a) specimen 1#; (b) specimen 2#.

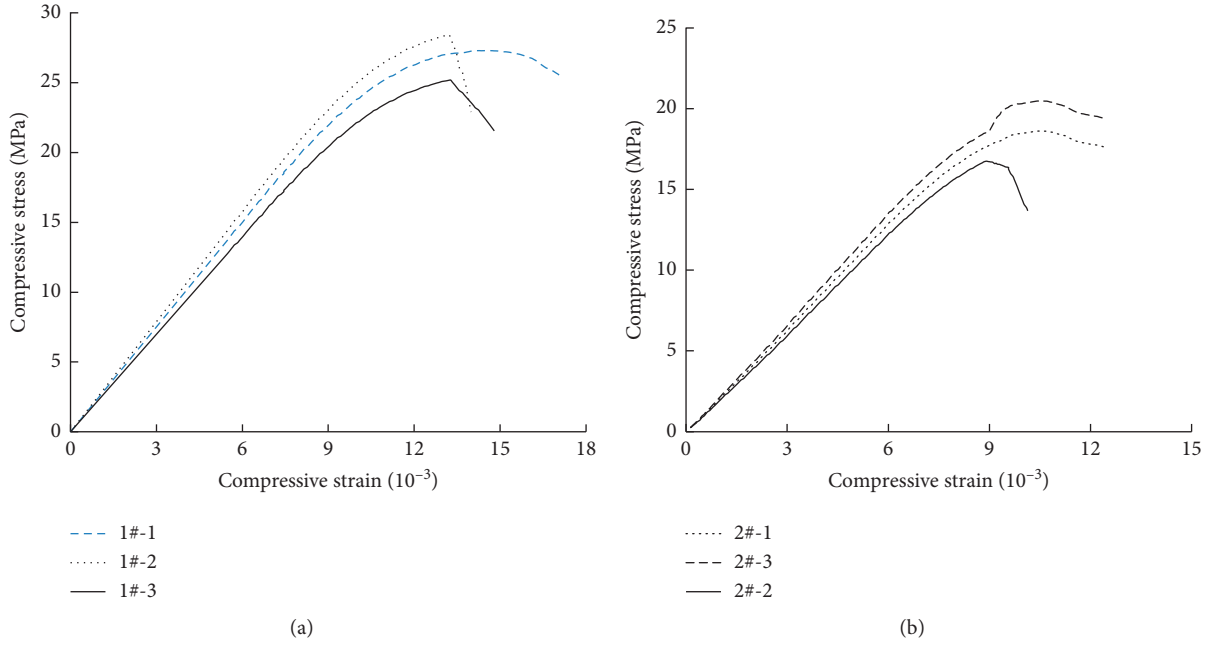

Figure 15: Compressive property of pervious concrete: (a) specimen 1#; (b) specimen 2#.

Figure 15 shows the stress-strain relationships of the pervious concrete specimens 1# and 2#. The test results show that as the stress increases, the strain of specimens increases linearly at the beginning stage. The mechanical property at this stage is elastic which is similar to that of common impervious concrete. As the loads continued to increase, microcracks initiated and propagated, resulting in a decrease of the stress-strain curve slope. The average compressive strength of specimen 1# is 26.2 MPa which is much higher than that of specimen 2#. The latter average compressive strength is 18.3 MPa. The difference is induced by the different porosities in the specimens. The pores are the weak parts in pervious concrete and distress may appear around the pores. Normally, the higher the porosity, the lower the compressive strength. In this test, the average porosity of specimen 1# is 21.9% and the average porosity of specimens 2# is 27.3%. Thus, it can be concluded that porosity has an important influence on the mechanical properties of pervious concrete.

3.4.2. Composition Modulus Determination. In pervious concrete, aggregates are bonded by cement paste. The modulus of aggregate-cement paste is affected by the aggregate modulus, the cement content, and the bond strength of cement paste. The composite modulus reflects the

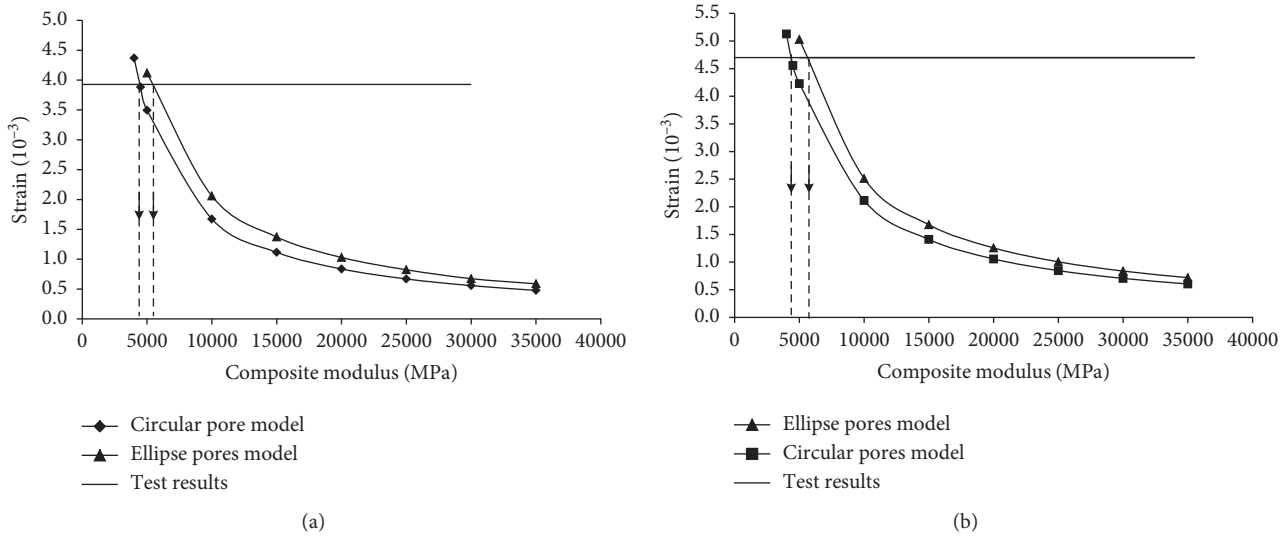

Figure 16: Composite modulus of aggregate-cement paste determination in simulation model: (a) specimen 1#; (b) specimen 2#.

composite mechanical property of an aggregate-cement paste material. To determine a reasonable modulus, the composite modulus varies widely from 3,000 to 35,000 MPa, and the compressive stress of 10 MPa is applied on top surface of the simulation models. The relationships between the vertical strain and the composite modulus have been calculated and the results are shown in Figure 16. In addition, the measured strain corresponding to the compressive stress of 10 MPa can be obtained by the laboratory test data (Figure 15). Based on the comparative method, the intersection of the test results and the simulation results can be obtained in Figure 16 and the corresponding composite modulus in horizontal axis can be also obtained. In Figure 16(a), the composite moduli of specimen 1# are 4,200 MPa and 5,500 MPa for the circular pore model and the elliptical pore model, respectively. Similarly, the composite moduli of specimen 2# are 4,500 MPa and 5,900 MPa for the circular pore model and the elliptical pore model, respectively (Figure 16(b)). From these results, it can be seen that the composite modulus of aggregate-cement paste for pervious concrete is much smaller than that of impervious concrete. The composite modulus of the aggregate-cement paste of the pervious concrete in the simulation model can be chosen within the range of 4,000 to 6,000 MPa according to the porosity of pervious concrete.

4. Conclusions

In this study, a random pore FEM has been developed to simulate the mechanical property of pervious concrete. In the simulation model, the influence of pore characteristics, including porosity, shape, and pore size, has been considered and the determination of the composite modulus of the aggregate-cement paste has also been discussed. The conclusions are as follows:

(1) The random pore FEM can be used to simulate the real pore features, including the size, shape, and random distribution. In addition, the aggregate and cement paste has been simplified into one composite material which can significantly improve the efficiency in the model meshing, calculations, and result extracting.

(2) The distribution and size of pores have an important effect on the stress distribution of pervious concrete. If the distance between bigger pores is small, the stress around the pores may be high. For instance, when the horizontal distance between two big pores is small, the compressive stress between the pores is very large. In another case, when the vertical distance between two big pores is small, the tensile stress between the pores is very high. In these cases, microcracks or damage may occur around the pores.

(3) In the random pore FEM, ellipse and roundness have been used to characterize the features of real pores. The method can describe the shape and size of actual pores. In particular, the inclined angle of pores can be also represented by adjusting the degree of long axis or short axis of the ellipse. The simulation results show that the stress and strain in the random elliptical pore model are larger than those in the random circular pore model. This is induced by the difference in the stress concentration around circular and elliptical pores.

(4) The composite modulus of aggregate-cement paste is an important parameter in the simulation model, which affects the accuracy of simulation results. By comparing the simulation results and the test data, a reasonable composition modulus for pervious concrete has been obtained. In this study, the composite modulus of aggregate-cement paste varies from 4,000 MPa to 6,000 MPa for the pervious concrete with porosity of 20%~30%. It is noticed that the value of composite modulus is remarkably lower than that of common cement concrete.

Data Availability

The data supporting the conclusions of the present study can be obtained from the corresponding author.

Conflicts of Interest

The authors declare that they have no conflicts of interest.

Authors' Contributions

J.S. and J.L. conceptualized the study and were involved in original draft preparation; J.S. contributed to methodology, performed formal analysis, and was involved in project administration; J.L. was responsible for software and resources; J.L. and F.L. were involved in validation, performed data curation, and contributed to funding acquisition; F.L. contributed to investigation.

Acknowledgments

This research was funded by "A Project of Shandong Province Higher Educational Science and Technology Program," grant number J17KA213.

References

[1] B. Debnath and P. P. Sarkar, "Permeability prediction and pore structure feature of pervious concrete using brick as aggregate," *Construction and Building Materials*, vol. 213, pp. 643–651, 2019.

[2] C.-W. Tang, C.-K. Cheng, and C.-Y. Tsai, "Mix design and mechanical properties of high-performance pervious concrete," *Materials*, vol. 12, no. 16, p. 2577, 2019.

[3] J. Ajayshankar and G. P. Ong, "Development of discharge–based thresholding algorithm for pervious concrete pavement mixtures," *Materials in Civil Engineering*, vol. 31, Article ID 04019179, 2019.

[4] H. Rifai, A. Staude, D. Meinel, B. Illerhaus, and G. Bruno, "In-situ pore size investigations of loaded porous concrete with non-destructive methods," *Cement and Concrete Research*, vol. 111, pp. 72–80, 2018.

[5] L. K. Crouch, J. Pitt, and R. Hewitt, "Aggregate effects on pervious Portland cement concrete static modulus of elasticity," *Journal of Materials in Civil Engineering*, vol. 19, no. 7, pp. 561–568, 2007.

[6] H. Zhou, H. Li, A. Abdelhady, H. X. Liang, B. Wang, and B. Yang, "Experimental investigation on the effect of pore characteristics on clogging risk of pervious concrete based on CT scanning," *Construction and Building Materials*, vol. 212, pp. 130–139, 2019.

[7] M. S. Sumanasooriya and N. Neithalath, "Pore structure features of pervious concretes proportioned for desired porosities and their performance prediction," *Cement and Concrete Composites*, vol. 33, no. 8, pp. 778–787, 2011.

[8] N. Neithalath, M. S. Sumanasooriya, and O. Deo, "Characterizing pore volume, sizes, and connectivity in pervious concretes for permeability prediction," *Materials Characterization*, vol. 61, no. 8, pp. 802–813, 2010.

[9] A. K. Chandrappa and K. P. Biligiri, "Comprehensive investigation of permeability characteristics of pervious concrete: a hydrodynamic approach," *Construction and Building Materials*, vol. 123, pp. 62716–6, 2016.

[10] T. Chen, Y. Luan, T. Ma, J. Zhu, X. Huang, and S. Ma, "Mechanical and microstructural characteristics of different interfaces in cold recycled mixture containing cement and asphalt emulsion," *Journal of Cleaner Production*, vol. 258, Article ID 120674, 2020.

[11] J. Zhang, Z. Fan, H. Wang, W. Sun, J. Pei, and D. Wang, "Prediction of dynamic modulus of asphalt mixture using micromechanical method with radial distribution functions," *Materials and Structures*, vol. 52, no. 2, p. 49, 2019.

[12] W. D. Martin III, B. J. Putman, and N. B. Kaye, "Using image analysis to measure the porosity distribution of a porous pavement," *Construction and Building Materials*, vol. 48, pp. 210–217, 2013.

[13] B. Rehder, K. Banh, and N. Neithalath, "Fracture behavior of pervious concretes: the effects of pore structure and fibers," *Engineering Fracture Mechanics*, vol. 118, pp. 1–16, 2014.

[14] R. Zhong and K. Wille, "Linking pore system characteristics to the compressive behavior of pervious concrete," *Cement and Concrete Composites*, vol. 70, pp. 130–138, 2016.

[15] J. Peng, J. Zhang, J. Li, Y. Yao, and A. Zhang, "Modeling humidity and stress-dependent subgrade soils in flexible pavements," *Computers and Geotechnics*, vol. 120, Article ID 103413, 2020.

[16] J. Leon Raj and T. Chockalingam, "Strength and abrasion characteristics of pervious concrete," *Road Materials and Pavement Design*, vol. 4, pp. 1–18, 2019.

[17] A. Ibrahim, E. Mahmoud, M. Yamin, and V. C. Patibandla, "Experimental study on Portland cement pervious concrete mechanical and hydrological properties," *Construction and Building Materials*, vol. 50, pp. 524–529, 2014.

[18] J. Zhang, L. Ding, F. Li, and J. Peng, "Recycled aggregates from construction and demolition wastes as alternative filling materials for highway subgrades in China," *Journal of Cleaner Production*, vol. 255, p. 120223, 2020.

[19] F. Tang, T. Ma, Y. Guan, and Z. Zhang, "Parametric modeling and structure verification of asphalt pavement based on BIM-ABAQUS," *Automation in Construction*, vol. 111, Article ID 103066, 2020.

[20] A. R. Mohamed and W. Hansen, "Micromechanical modeling of concrete response under static loading- part I: model development and validation," *ACI Materials Journal*, vol. 96, no. 2, pp. 196–203, 1999.

[21] W. Bo and G. Peng, "ANSYS implementation of Monte Carlo method for generating random aggregate model of concrete," *Journal of Shihezi University*, vol. 25, no. 04, pp. 504–507, 2007.

[22] Q. Dong, D. Yuan, B. Song, and Q. Cai, "Fractal verification of randomness of concrete mesoscopic aggregate model," *Journal of Hohai University*, vol. 39, no. 01, pp. 95–98, 2011.

[23] R. Li, Q. Li, J. Wei, G. Zhong, and Y. Xu, "Study on pore model of porous concrete," *Journal of Wuhan University of Technology*, vol. 31, no. 19, pp. 11–15, 2009.

[24] E. A. B. Koenders and K. van Breugel, "Numerical modelling of autogenous shrinkage of hardening cement paste," *Cement and Concrete Research*, vol. 27, no. 10, pp. 1489–1499, 1997.

[25] J. C. Walraven and H. W. Reinhardthw, "Theory and experiments on the mechanical behavior of cracks in plain and reinforce concrete subject to shear loading," *Heron*, vol. 26, no. 1A, pp. 26–35, 1981.

[26] E. Schlangen and J. G. M. van Mier, "Simple lattice model for numerical simulation of fracture of concrete materials and

structures," *Materials And Structures*, vol. 25, no. 9, pp. 534–542, 1992.

[27] J. G. M. Van Mier, *Fracture Processes of Concrete-Assessment of Material Parameters for Fracture Models*, CRC Press, Boca Raton, FL, USA, 1997.

[28] Ministry of Housing and Urban-Rural Development of the Peoples Republic of China, *CJJ/T135-2009, Technical Specifications for Pervious Concrete Pavement*, Architecture & Building Press, Beijing, China, 2009.

[29] ASTM C1688/C1688M-14a, *Standard Test Method for Density and Void Content of Freshly Mixed Pervious Concrete*, 2014.